[2]L. Knopoff, J. Geophys. Res. 13, 1 (1967).
[3]Don L. Anderson and C. Sammis, California Institute of Technology, Contribution No. 1547, Pasadena, 1968 (unpublished).
[4]I. A. Lambert and P. J. Wyllie, Nature 219, 1240 (1968).
[5]*Rare Metals Handbook*, edited by C. A. Hampel (Reinhold, New York, 1961). New York, 1961).
[6]Y. Eckstein, A. W. Lawson, and D. H. Reneker, J. Appl. Phys. 31, 1534 (1960).
[7]P. W. Bridgman, in *The Physics of High Pressure*, 2nd ed. (G. Bell, London, 1949).
[8]P. W. Bridgman, Proc. Am. Acad. Arts Sci. 81, 165 (1952).
[9]H. T. Hall, Rev. Sci. Instr. 31, 125 (1960).
[10]Shogo Matsushima, Geophys. Res. Inst. Kyoto 35, 117 (1965), special contribution.
[11]W. Klement, A. Jayaraman, and G. C. Kennedy, Phys. Rev. 131, 632 (1963).
[12]J. S. Kasper, R. H. Wilson, and R. Lewinki, Aeronautical Systems Division Technical Report No. 61-21, Part II, 1961 (unpublished).
[13]V. P. Butuzov. M. G. Gonikberg, and S. P. Smirnov, Dokl. Akad. Nauk SSSR 89, 651 (1953) [NSF Report No. tr-76 (unpublished)].
[14]P. W. Bridgman, Phys. Rev. 6, 1 (1915); 6, 94 (1915).
[15]M. L. McDaniel, S. E. Babb, Jr., and G. J. Scott, J. Chem. Phys. 37, 822 (1962).
[16]M. B. Gitis and I. G. Mikhailov, Akust. Zh. 11, 434 (1965) [Soviet Phys. Acoust. 11, 372 (1966)].
[17]O. J. Kleppa, J. Chem. Phys. 18, 1331 (1950).
[18]H. Richter and H. Oehme, Z. Naturforsch. 229, No. 5, 655 (1967).
[19]L. Hall, Phys. Rev. 71, 318 (1947).
[20]J. D. Dudley and H. T. Hall, Phys. Rev. 118, 1211 (1960).
[21]H. R. Thresh, A. F. Crawley, and D. W. G. White, Trans. AIME 242, 819 (1968).
[22]H. Krebs, H. Hermsdorf, H. Thurn, H. Welte, and L. Winkler, Z. Naturforsch. 23a, 491 (1968).
[23]E. G. Ponyatovskii, Fiz. Metal Metalloved. 16, 622 (1963).
[24]W. P. Mason, in *Physical Acoustics and the Properties of Solids* (Van Nostrand, Princeton, N. J., 1958), pp. 40–96.
[25]G. L. Kehl, in *Principles of Metallographic Laboratory Practice* (McGraw-Hill, New York, 1949).
[26]P. Dandekar, Ph.D dissertation (University of Chicago, 1967) (unpublished).
[27]P. Dandekar, Phys. Rev. 172, 873 (1968).
[28]*Metals Handbook*, edited by T. Lyman (American Society for Metals, Cleveland, Ohio, 1948).
[29]H. Mizutani and H. Kanamori, Japan. J. Phys. Earth XII, No. 2, 43 (1964).
[30]M. Kumazawa, H. Furiyashi, and K. Iida, Bull. Volcanol. Soc. Japan 9, No. 1, 1 (1964).

PHYSICAL REVIEW A VOLUME 3, NUMBER 5 MAY 1971

Phonon Dispersion Relations for hcp He^4 at a Molar Volume of 16 cm^3 *

R. A. Reese, S. K. Sinha, T. O. Brun, and C. R. Tilford
Institute for Atomic Research and Department of Physics, Iowa State University, Ames, Iowa 50010
(Received 15 October 1970)

The phonon spectrum of hcp He^4 has been measured along the three principal symmetry axes by inelastic neutron scattering from a single crystal with a molar volume of 16.00 cm^3 at 4.2 K. The results are in fair agreement with the theoretical calculations of Gillis, Koehler, and Werthamer, the maximum discrepancy being about 30%. Considerable phonon damping has been observed for the Δ_2(LO) and Σ_3($TO_\perp$) branches. A modified axially symmetric force-constant model has been fitted to the dispersion curves and used as an interpolation scheme to calculate the frequency distribution function and other thermodynamic functions.

I. INTRODUCTION

The properties of quantum crystals have been the subject of considerable interest over the last few years. Theoretical efforts in this field have led recently to sophisticated theories predicting the dynamical properties of such systems. Until recently, the lack of experimental data on oriented single crystals of such solids has necessitated a comparison of the theoretical predictions with only the bulk properties of such systems. The unique feature associated with quantum crystals is the fact that the zero-point energy accounts for a large fraction of the total energy of the crystal. The solids which exhibit quantum-crystal behavior most strongly are the crystalline forms of He^3 and He^4. This is due to the low masses of the helium atoms and the weak binding forces between them, which give rise to large-amplitude zero-point vibrations of the atoms about their equilibrium positions. Since the amplitudes become comparable to the interatomic spacings, it is obvious that such a system is likely to be highly anharmonic, and furthermore that the short-range correlations between the atoms have to be considered carefully. In fact, as is well known, a purely harmonic calculation predicts imaginary fre-

quencies for such systems. The theory for treating these systems has been extensively referenced in a recent review paper by Werthamer.[1] The most recent formalism for calculating phonon frequencies in helium is the self-consistent phonon theory of Koehler[2] as then calculated by Gillis, Koehler, and Werthamer[3] (GKW), which includes the short-range correlation functions introduced by Nosanow.[4] The self-consistent phonon theory is discussed in more detail in Sec. IV.

In the last few years, several experiments on single-crystal specimens of hcp He^4 have yielded much more detailed information about this solid. Measurements made on single crystals of hcp He^4 include optical birefringence measurements,[5] thermal conductivity measurements,[6,7] elastic constant measurements,[8] and determinations of the phonon spectrum using inelastic neutron scattering.[9-11] The phonon spectrum has been measured at a molar volume of 21.1 cm^3 by the Brookhaven group[9] and at 16.0 cm^3 by us. Some preliminary results of our own measurements were reported earlier.[10] Neutron scattering measurements on polycrystalline hcp He^4 at a molar volume of 20.9 cm^3 have also been reported.[11] We report here on a more complete set of results for the phonon-dispersion curves along the symmetry directions of hcp He^4 at the 16.00 cm^3 molar volume. The neutron scattering measurements of the phonon spectrum in solid helium are beset by considerable difficulties, among which are the small coherent neutron cross section (0.73 b) for the He^4 nucleus, the large amplitude of oscillation, resulting in a severe attenuation of scattered intensity due to the Debye-Waller factor, and the consequent need for growing and maintaining over long periods of time a large and suitably oriented single crystal. Our choice of molar volume was determined by the decision to grow the crystal at a molar volume at which the crystalline phase could be maintained at 4.2 K. It was decided to grow the crystal at a pressure of 230 bar corresponding to a melting temperature of 5.4 K. Additional advantages of working at this molar volume are that the Debye temperature is about 50 K, so that the phonon frequencies are not inconveniently small, and the attenuation in the scattered neutron intensities due to the Debye-Waller factor, although severe, still permits measurements to be made over a reasonable range in reciprocal space. It is perhaps fortunate that measurements in this solid exist for such widely varying molar volumes as 16.00 and 21.1 cm^3, making helium the only solid for which the phonon spectrum has been measured for such differing densities in the same crystalline phase. This also provides a direct test of the theoretical predictions for the density dependence of the phonon spectrum, which is particularly difficult to calculate because of the need to know accurately the short-range correlations between the helium atoms. As will be discussed in Sec. IV, the 16.0 and 21.1 cm^3 molar-volume data together provide a rather complete picture of the phonon-dispersion curves over a wide range of molar volumes. This is also borne out by the good agreement between the Grüneisen parameter obtained from the neutron measurements with that obtained from thermodynamic data.

Our measurements have also revealed some of the inadequacies of the current theories by demonstrating the existence of lifetime effects for a number of phonon branches.

II. EXPERIMENTAL TECHNIQUE

The helium crystal was grown in a stainless-steel container which was pressurized through a stainless-steel capillary to a pressure of 230 bar. This pressure was generated by a thermal pump consisting of two pressure vessels which were alternately cooled and warmed between 77 and 300 K. No contamination was thereby introduced. The sample container was 50 mm long and had an o.d. of 12.7 mm and a wall thickness of 0.25 mm. Stainless steel was used instead of aluminum in spite of its large neutron cross section because of the need to have the container walls possess as low a thermal conductivity as possible. Heater coils and thermocouples were attached to the top and bottom of the container so that a temperature gradient could be maintained across it. The crystals were grown by slowly cooling the bottom and the top of the container, maintaining the bottom at a temperature of about 0.1 K below the top. During solidification, the pressure in the container was maintained constant by keeping the capillary open by means of heater coils, and when the whole container was filled with solid, the capillary was allowed to cool to 4.2 K, thereby sealing off the container and allowing all processes after that to take place at constant volume only. The container was tapered at the bottom in the hope that a single grain would grow through the constriction and fill the container. In fact, the solidification process alone was never observed to yield a single crystal, but rather produced several large grains filling the container. About 24 h after solidification, the solid was annealed by bringing the top of the container to within a few millidegrees of the melting point, while maintaining a temperature differential of 50 mdeg for a period of about 12 h. Occasionally this procedure would yield a very large single crystal which was then slowly cooled to 4.2 K and used for the measurements. The complete series of measurements reported in this paper, which span a time period of several months, were performed on four such different crystals, the largest having a volume of 5 cm^3 and filling the whole con-

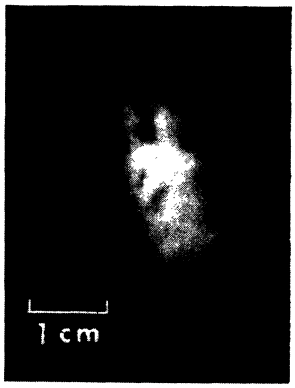

FIG. 1. Photograph of the helium crystal used in most of the measurements taken by Bragg reflection of neutrons.

tainer. The cryostat containing the sample was mounted on a two-circle goniometer which could rock the crystal about two perpendicular axes by ± 30° as well as rotate it about a vertical axis.

The crystal shapes and orientations were found by neutron diffraction, i.e., by setting the detector arm approximately for Bragg reflection from a particular set of planes and rotating and rocking the goniometer until a reflection had been found. The Bragg-reflected neutron beam was photographed using a Polaroid neutron camera. Such a photograph of the 5-cm^3 crystal is shown in Fig. 1. It was found that the crystals generally tended to grow with the c axis normal (within about 15°) to the long axis of the container, i.e., normal to the growth direction. Once a crystal had been found, it was oriented so that the plane of scattering was a symmetry plane (i.e., a b^*-c^* or a^*-c^* plane) and the rest of the container masked off with cadmium. The lattice constants of the crystal used for most of the measurements were determined to be $a = 3.3535 \pm 0.002$ Å, $c = 5.4636 \pm 0.002$ Å, and hence the molar volume $V_m = 16.02 \pm 0.03$ cm^3. Some of the runs were made on a crystal with a slightly differing molar volume ($V_m = 16.58$). The way these results are normalized to those for the other crystal is discussed below.

The inelastic scattering measurements were made using the triple-axis spectrometer at the Ames Laboratory Research Reactor. The "constant-Q" mode of scanning with fixed incident energy was used throughout. Two incident energies, 18.6 and 20.4 MeV, were used for most of these measurements.

At 4.2 K, the only appreciable one-phonon cross section corresponds to a process in which the neutron excites a quantum of vibrational energy in the crystal. The differential cross section for a one-phonon neutron energy-loss process is given by

$$\frac{d^2\sigma}{d\Omega\, d\epsilon} \propto \frac{k'}{k}\left(1+\frac{1}{e^{\hbar\omega/kT}-1}\right)e^{-2W}g_j^2(\vec{Q}), \qquad (1)$$

where ω is the phonon frequency, T the temperature, and W is the Debye-Waller factor, which for a hcp crystal is given by

$$2W = \frac{\hbar^2}{2M}\left[\frac{Q_\parallel^2}{k\Theta_0}G_\parallel\left(\frac{T}{\Theta_0}\right)+\frac{Q_\perp^2}{k\Theta_0}G_\perp\left(\frac{T}{\Theta_0}\right)\right], \qquad (2)$$

where M is the atomic mass, Θ_0 is the Debye temperature at 0 K, $Q_\parallel$ and $Q_\perp$ are, respectively, the components of the neutron scattering vector $\vec{Q}$ parallel and perpendicular to the basal plane, and $G_\parallel$ and $G_\perp$ are dimensionless functions of T/Θ_0 which depend on the phonon spectrum.

Finally, $g_j(\vec{Q})$ in Eq. (1) is the inelastic structure factor defined by

$$g_j^2(\vec{Q}) = \left|\sum_\kappa \frac{b\vec{Q}\cdot\vec{e}_{\kappa,j}(\vec{q})}{[M\omega_j(\vec{q})]^{1/2}}\, e^{i\vec{Q}\cdot\vec{r}_\kappa}\right|^2, \qquad (3)$$

where b is the coherent nuclear scattering length for the He^4 nucleus, $\omega_j(\vec{q})$ and $\vec{e}_{\kappa,j}(\vec{q})$ are, respectively, the frequency and polarization vector associated with the jth branch and κth atom in the unit cell for phonon wave vector $\vec{q}$, and $\vec{r}_\kappa$ is the position of the κth atom in the unit cell.

Normally, the factor e^{-2W} varies very slowly in reciprocal space and does not affect the intensities of the scattered neutron groups seriously. However, for He^4, the large-amplitude zero-point oscillations cause the factor e^{-2W} to die away sufficiently rapidly with increasing Q so as to overcome the Q^2 factor in $g_j^2(\vec{Q})$ at values of Q which are comparable to the distances of the first few reciprocal-lattice points. Figure 2 shows the function Q^2e^{-2W} together with the same function calculated for a Θ_0 of 25 K appropriate to the 21.1-cm^3 molar volume studied by the Brookhaven group. Although it may be seen that a greater range in reciprocal space is obtained at the 16.00-cm^3 molar volume, nevertheless, one sees that only a few reciprocal-lattice points are available from which to pick up the phonon branches.

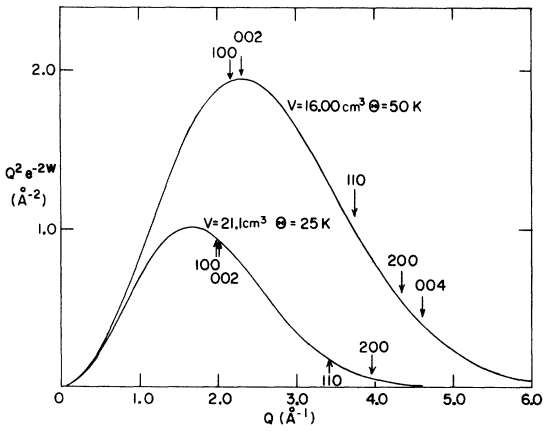

FIG. 2. Function Q^2e^{-2W} for hcp He^4 at molar volumes of 16.00 and 21.1 cm^3.

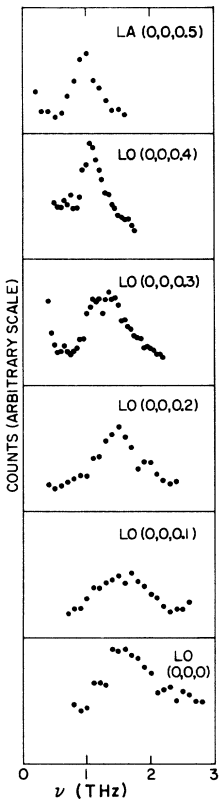

FIG. 3. Observed neutron groups corresponding to longitudinal phonons along Δ.

III. RESULTS

Measurements were made of the dispersion curves along the principal symmetry axes of the reciprocal lattice. These are the $\Gamma A[0001]$, $\Gamma M[10\bar{1}0]$, and $\Gamma KM[11\bar{2}0]$ axes. Neutron groups were studied corresponding to the Δ_1(LA), Δ_2(LO), Δ_5(TA), and Δ_6(TO) branches in the ΓA direction, the Σ_1(LA and LO), Σ_3($TA_\perp$ and $TO_\perp$) branches in the Γ direction, and the $T_3(TA_\perp)$ branches in the ΓKM direction. Because the crystal could never be oriented so that the c axis was normal to the scattering plane, it was not possible to study the Σ_4($TA_\parallel$ and $TO_\parallel$) branches in the ΓM direction. Figure 3 shows a set of neutron groups corresponding to some of the phonons along the Δ_1 and Δ_2 branches. It may be observed that the neutron groups are reasonably well defined for the Δ_1(LA) branch but show considerable broadening for the Δ_2(LO) branch with increasing phonon frequency. Along the ΓM direction, well-defined neutron groups were observed corresponding to the Σ_3 ($TA_\perp$) branches and to the Σ_1 (LA and LO) branches, but only very poorly defined neutron groups could be observed for the $\Sigma_3(TO_\perp)$ branch. These latter neutron groups are not included in the main body of the results but are discussed separately in Sec. IV. For the ΓKM direction, well-defined groups were obtained for the $T_3(TA_\perp)$ branch. For the $T_2(TO_\perp)$ branch only the point at M was measured. The measured phonon frequencies are tabulated in Table I.

Figure 4 shows the measured dispersion curves. Also shown are the Σ_3 branches along ΓM which were obtained by scaling the Brookhaven data (21.1-cm^3 molar volume). The justification for such a scaling procedure is given below. It may be seen that the dispersion curves for hcp He^4 seem to exhibit considerable acoustic isotropy, as witnessed by the near equality of the initial slopes of the longitudinal acoustic branches along ΓA and ΓM and the near equality of the initial slopes of the $TA_\parallel$ and $TA_\perp$ modes along ΓM. In this respect they are similar to the dispersion curves for other hcp solids with a near ideal c/a ratio.[12] On the other hand, the

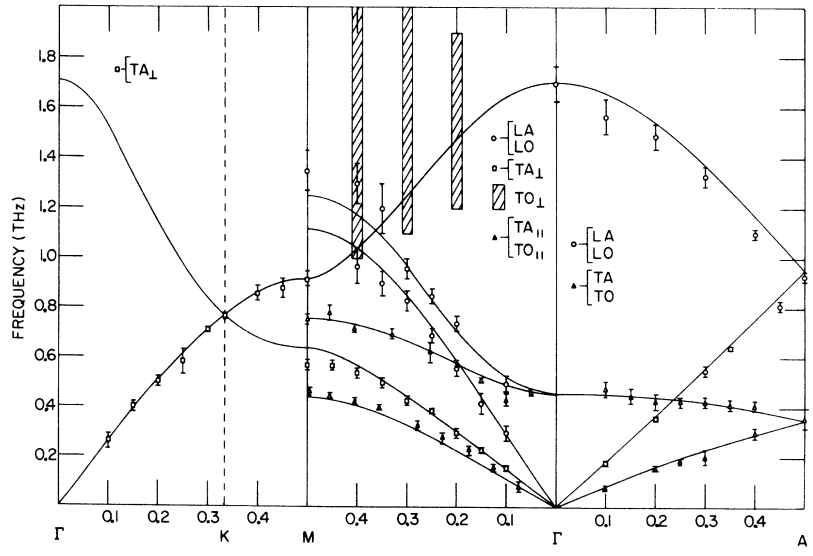

FIG. 4. Phonon-dispersion curves for hcp He^4 at $V_m = 16.00$ cm^3. $TA_\parallel$ and $TO_\parallel$ branches along ΓM were obtained by scaling the Brookhaven data from $V_m = 21.1$ cm^3. Shaded areas along ΓM correspond to the anomalous neutron groups observed and referred to in the text. The smooth curves are obtained from the 18-parameter force-constant model fitted to the data.

TABLE I. Measured phonon frequencies in hcp He^4 at $V_m = 16.00$ cm^3 and $T = 4.2$ K.

ζ	ν(THz)	ζ	ν(THz)
$\vec{q} = (0, 0, \zeta)2\pi/c$			
Δ_1(LA)		Δ_2(LO)	
0.10	0.18 ± 0.01	0.00	1.70 ± 0.07
0.20	0.36 ± 0.01	0.10	1.57 ± 0.07
0.30	0.55 ± 0.02	0.20	1.49 ± 0.05
0.35	0.64 ± 0.01	0.30	1.33 ± 0.04
0.45	0.81 ± 0.02	0.40	1.10 ± 0.02
0.50	0.93 ± 0.02	0.50	0.93 ± 0.02
Δ_5(TA)		Δ_6(TO)	
0.10	0.08 ± 0.01	0.10	0.48 ± 0.03
0.20	0.17 ± 0.01	0.15	0.45 ± 0.03
0.25	0.19 ± 0.01	0.20	0.43 ± 0.03
0.30	0.20 ± 0.03	0.25	0.43 ± 0.02
0.40	0.30 ± 0.02	0.30	0.42 ± 0.02
0.50	0.36 ± 0.04	0.35	0.42 ± 0.02
		0.40	0.41 ± 0.02
		0.50	0.36 ± 0.04
	$\vec{q} = (\zeta, 0, 0)4\pi/\sqrt{3}a$		
Σ_1(LA)		Σ_1(LO)	
0.10	0.30 ± 0.03	0.10	0.55 ± 0.03
0.15	0.42 ± 0.04	0.20	0.74 ± 0.03
0.20	0.56 ± 0.03	0.25	0.85 ± 0.03
0.25	0.69 ± 0.03	0.30	0.96 ± 0.04
0.30	0.83 ± 0.04	0.35	1.20 ± 0.10
0.35	0.90 ± 0.05	0.40	1.30 ± 0.08
0.40	0.97 ± 0.07	0.50	1.35 ± 0.08
Σ_3(TA$_\perp$)		Σ_4(TA$_\parallel$)	
0.10	0.16 ± 0.01	0.076	0.09 ± 0.02[a]
0.15	0.23 ± 0.01	0.126	0.16 ± 0.015[a]
0.20	0.30 ± 0.02	0.177	0.23 ± 0.015[a]
0.25	0.39 ± 0.01	0.227	0.28 ± 0.02[a]
0.30	0.43 ± 0.02	0.278	0.33 ± 0.02[a]
0.35	0.50 ± 0.02	0.354	0.402 ± 0.005[a]
0.40	0.54 ± 0.02	0.404	0.42 ± 0.015[a]
0.45	0.57 ± 0.02	0.455	0.45 ± 0.01[a]
0.50	0.57 ± 0.02	0.494	0.47 ± 0.015[a]
		Σ_4(TO$_\parallel$)	
		0.050	0.48 ± 0.01[a]
		0.101	0.43 ± 0.02[a]
		0.152	0.52 ± 0.005[a]
		0.202	0.57 ± 0.01[a]
		0.253	0.62 ± 0.04[a]
		0.329	0.70 ± 0.02[a]
		0.404	0.72 ± 0.015[a]
		0.455	0.78 ± 0.03[a]
		0.500	0.75 ± 0.02[a]
	$\vec{q} = (\zeta, \zeta, 0)4\pi/a$		
		T_3(TA$_\perp$)	
		0.10	0.26 ± 0.03
		0.15	0.04 ± 0.02
		0.20	0.50 ± 0.02
		0.25	0.58 ± 0.05
		0.30	0.71 ± 0.01
		0.333	0.77 ± 0.01
		0.40	0.86 ± 0.03
		0.45	0.88 ± 0.04
		0.50	0.92 ± 0.03

[a]Brookhaven data scaled by 1.91.

ratio of the two optic-mode frequencies at Γ is quite large (~4) compared to about 1.7 for hcp metals with similar c/a ratios.

We have also studied phonon lifetime effects by extracting the instrumental resolution from the observed widths of the neutron groups. Using the formalism of Cooper and Nathans,[13] the resolution function was calculated by approximating the dispersion surfaces in the vicinity of the observed points by planes. The errors in such a procedure might be expected to be large, owing to statistical uncertainties in the observed linewidths and possible errors in the calculated resolution function. Nevertheless, we conclude from our results that within experimental error no broadening was observed for the TA$_\perp$ branches along ΓM and ΓKM. The natural phonon linewidths of the Σ_1 branches could not be measured due to contamination of one branch by the other, but we place an upper limit of 0.40 THz on the natural full width at half-maximum (Γ_{ph}) of the phonons in these branches. As far as the ΓA direction is concerned, the TA branch exhibits no detectable broadening, and we place an upper limit of $\Gamma_{ph} = 0.2$THz on the TO branch. A more accurate determination for these branches was precluded by contamination due to elastic scattering and the small linewidths involved. Natural broadening, however, is most clearly demonstrated by the behavior of the LA and LO branches along ΓA. These are in many cases sufficiently broadened for the natural linewidths to be determined with some confidence, and Fig. 5 shows the behavior of Γ_{ph} for the LA and LO branches plotted together in the double-zone representation. These results show that for the highest frequencies the phonons corresponding to this branch are not well-defined excitations, because the ratio ν/Γ_{ph}, which is a rough measure of the number of oscillations before the phonon decays, is only about 2.

IV. DISCUSSION

The most striking feature about the comparison between the two sets of data at molar volumes of 16.00 and 21.1 cm^3 is that all the frequencies scale by approximately the same factor. Table II lists a ratio of the frequencies of selected modes for the two molar volumes. Where the phonons were not measured at precisely the same wave vector, we have interpolated our data to obtain the above ratios. It may be seen that this ratio is indeed approximately constant for all these modes to within a maximum discrepancy of 14%. We have chosen the ratio of the frequencies for ΔLA at $\vec{q} = 2\pi/c\,(0, 0, 0.475)$, which is 1.91 as the scaling factor for the 21.1-cm^3 data relative to ours, since these particular frequencies have the smallest percentage errors associated with them. Using this scaling factor we have obtained the presumed dispersion curves for the Σ_4 (TA$_\parallel$ and TO$_\parallel$) branches at our molar volume,

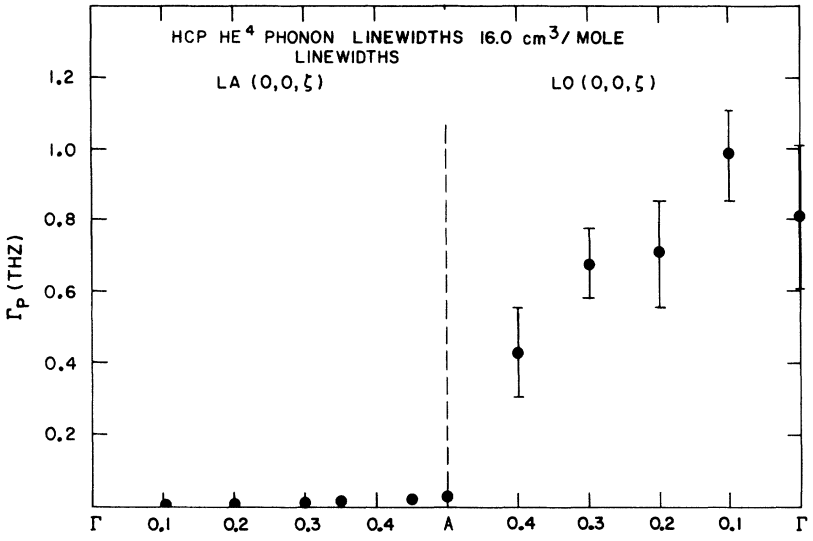

FIG. 5. Natural full width at half-maximum of phonons for the longitudinal branches along Δ.

which we have then combined with our other data and used for further analysis. One check of the validity of this procedure is that at the point M, the $\Sigma_4(\mathrm{TA}_{\parallel})$ branch joins up with the longitudinal mode propagating along the ΓKM direction. We have measured the frequency of this particular mode at the point M and the ratio of this frequency to the 21.1-cm^3 molar-volume frequency for $\Sigma_4(\mathrm{TA}_{\parallel})$ at M is 1.76, implying that at the zone boundary, at least, the scaling law is approximately obeyed for this branch.

In view of the scaling of the frequencies, the Grüneisen parameter γ_i defined as $(-d\ln\omega_i/d\ln V)$ for the ith normal mode is approximately the same for all modes and must therefore be close to the γ for the bulk solid, without involving the troublesome averages over normal modes which have to be carried out for most solids. Existing data regarding γ from specific-heat and $(\partial P/\partial T)_V$ measurements,[14] as well as thermodynamic arguments,[15] suggest that the volume dependence of γ may be approximately represented by a linear relationship of the form

$$\gamma = \alpha V_m . \tag{4}$$

If we assume Eq. (4) is true, then a simple integration yields the following relation between the frequencies at molar volumes V_m^1 and V_m^2:

$$\ln(\omega_2/\omega_1) = \alpha(V_m^1 - V_m^2). \tag{5}$$

Putting in the values for the 16.00- and 21.1-cm^3 molar volumes, we obtain $\alpha = 0.1262$ cm^{-3}, from which the values of γ at the two molar volumes may be obtained from Eq. (4) as $\gamma(V_m = 16.00\ \mathrm{cm}^3) = 2.02$, and $\gamma(V_m = 21.1\ \mathrm{cm}^3) = 2.66$. The above values have neglected a possible variation of γ with temperature, because we are comparing frequencies measured at a temperature of 4.2 K ($V_M = 16.00$ cm^3) with those measured at 1.0 K ($V_m = 21.1$ cm^3). Nevertheless, for comparison with the γ's obtained from bulk measurements, we may see that using Eq. (4) our data interpolate to $\gamma(V_m = 19.00\ \mathrm{cm}^3) = 2.4$, which is to be compared with a γ of 2.6 ± 0.05 at $V_m = 19.00$ cm^3 at a temperature of 1.5 K obtained from bulk measurements.[14] A further check for the consistency of our value for γ at $V_m = 16.00$ cm^3 and 4.2 K is the fact that, as mentioned in Sec. II, some measurements were made on a crystal which grew at $V_m = 16.58$ cm^3. The frequency of the longitudinal mode at A was measured for both the 16.00- and 16.58-cm^3 molar volumes to an accuracy of 2%. The results are

$$[\omega(V_m = 16.00\ \mathrm{cm}^3)]/[\omega(V_m = 16.58\ \mathrm{cm}^3)] = 1.08 ,$$

whereas using $\gamma = 2.02$, we calculate the ratio expected for these frequencies to be also 1.08.

To obtain a suitable interpolation scheme to be used for calculating the frequencies for the off-symmetry directions as well, we have used a modified axially symmetric (MAS) force-constant formalism.[16] A sixth-neighbor axially symmetric model was also tried, but found to be unsatisfactory,

TABLE II. Ratio of selected mode frequencies at $V_m = 16.0$ cm^3 and $V_m = 21.1$ cm^3.

Branch	$q/q_{\max}$	$\nu(16.0)/\nu(21.1)$
Δ_1(LA)	0.95	1.91 ± 0.17
Δ_5(TA)	0.76	1.91 ± 0.24
Δ_6(TO)	0.28	2.03 ± 0.22
$\Sigma_3(\mathrm{TA}_\perp)$	1.0	2.18 ± 0.14
Σ_1(LA)	0.56	2.04 ± 0.18
Σ_1(LO)	0.60	1.95 ± 0.18

compared to a seventh-neighbor MAS model. We conclude from this that it is necessary to include anisotropy between the c axis and the basal-plane constants. We do not imply, of course, that the force-constant parameters obtained from such a fit represent the actual interactions between atoms, since the harmonic approximation is inapplicable to this solid. In order to obtain a fit to the dispersion curves, the quantities $\sum_j \omega_j^2(\vec{q})$ (where j is summed over all branches belonging to the the same irreducible representation) were Fourier-analyzed to obtain interplanar force constants which are linear combinations of the atomic force constants. The procedure for doing this is described in detail in Ref. 12. The results showed that the interplanar force constants involving interactions parallel to the basal plane were consistent with interactions up to at least six nearest neighbors, whereas the interplanar force constants between the hexagonal layers required interactions parallel to the c axis which extended up to at least the third layer. Thus the MAS model used involved altogether 18 parameters which are the 17 MAS parameters referred to in Ref. 12, together with the force constant G_4 which refers to the zz interaction between the origin atom and its seventh neighbor. The notation is that of Czachor.[17] These 18 parameters were determined by performing a least-squares fit to the interplanar force constants, the elastic constants, certain frequencies at M, and the lowest branch at the point H in the Brillouin zone. These relations consisted of 27 linear equations and one quadratic equation, the latter resulting from the so-called "optical correction" to the expression for the elastic constant C_{11} in terms of the force constants. The elastic constants C_{11}, C_{66}, C_{44}, and C_{33} were obtained from the initial slopes of the measured dispersion curves. The elastic constant C_{13} cannot be determined from dispersion curves for symmetry directions, and accordingly we have taken C_{13} from the elastic constant measurements of Franck and Wanner[8] at $V_m = 20.9$ cm^3, after suitably scaling their data to our molar volume, using Eq. (5). The fit obtained to the dispersion curves using this 18-parameter model is shown together with the experimental points in Fig. 4. It may be seen that a good fit is obtained with this model; the maximum discrepancy occurs at M for the $\Sigma_3(\mathrm{TA}_\perp)$ branch and is of the order of 10%. The force-constant parameters obtained in this way are listed in Table III. It was found that the parameters a_1, b_1, g_1, a_2, b_2, g_2, a_3, b_3, g_3, G_1, G_2, G_3, and G_4 could not be varied appreciably without adversely affecting the goodness of the fit. However, the parameters A_1, B_1, A_2, B_2, A_3, and B_3, although very much interconnected, could be obtained in several equivalent sets to fit the data almost equally well.

It was necessary to include the frequency of the lowest branch at the point H in the Brillouin zone because the model gave a negative frequency at this point when the model was left unconstrained. Because a low frequency at the zone edge seemed unlikely, in the absence of experimental data at this point, the branch was constrained to have a frequency of 0.2 THz here. This corresponds to a temperature of 9.6 K and is sufficiently high that contributions to the specific heat from points near H will be negligible. This anomalous behavior at the point H was caused by a near cancellation of two large terms involving the G's and g's. Constraining the frequencies at H resulted in a slightly worse fit to some of the phonons along the symmetry directions.

We have used the model involving the parameters listed in Table III to calculate the frequency distribution function $g(\nu)$ using the technique of Raubenheimer and Gilat.[18] The resulting $g(\nu)$ is shown in Fig. 6. As indicated in the figure, most of the conspicuous critical points can be identified with the predictions of the model for the two optic modes at Γ and the zone-boundary modes at M. We have used this $g(\nu)$ to calculate the temperature dependence of the Debye Θ. This is shown in Fig. 7. Θ_0, which is the Debye Θ at 0 K, is obtained as 47.2 K, which is to be compared with the recent experimental value of 52 K obtained by Ahlers.[19] The theoretical curve dips to a minimum at $T = 3.4$ K, resulting from dispersion of the acoustic branches. The decrease in Θ with temperature is also observed in the specific-heat data; however, the minimum at 3.4 K is not reproduced. This may result from extra contributions to the specific heat as-

TABLE III. Force constants for the seven-neighbor MAS model. Units are dyn/cm.

Neighbor	GTF notation	MAS notation
	$A_1 = 7.678$	$\delta_1 = 0.271$
1	$B_1 = 7.136$	$\epsilon_{1x} = 46.342$
	$G_1 = 48.50$	$\epsilon_{1z} = 46.342$
	$a_1 = 15.72$	$\alpha_2 = 58.480$
2	$f_1 = 44.96$	$\beta_{2x} = 1.100$
	$g_1 = -25.52$	$\beta_{2z} = -25.520$
	$A_2 = -7.283$	$\delta_3 = 0.367$
3	$B_2 = -1.415$	$\epsilon_{3x} = -7.283$
	$G_2 = 8.881$	$\epsilon_{3z} = 5.961$
	$a_2 = 1.122$	$\beta_{4x} = 1.122$
4	$g_2 = -35.24$	$\alpha_4 + \beta_{4z} = -35.240$
	$A_3 = 0.5894$	$\delta_5 = 0.0852$
5	$B_3 = 0.9302$	$\epsilon_{5x} = -0.433$
	$G_3 = 2.169$	$\epsilon_{5z} = 1.491$
	$a_3 = -0.06737$	$\alpha_6 = -9.011$
6	$b_3 = -9.078$	$\beta_{6x} = -0.067$
	$g_3 = -1.713$	$\beta_{6z} = -1.713$
7	$G_4 = 1.831$	$\epsilon_{7z} = 1.831$

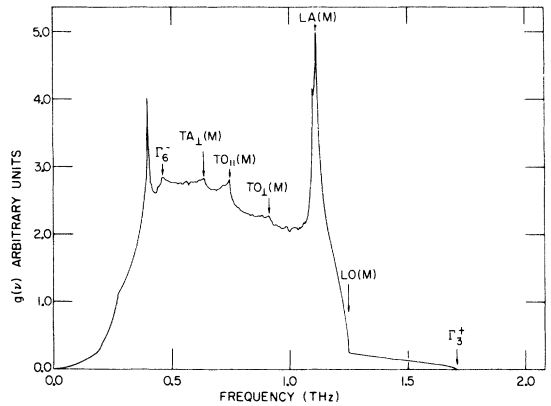

FIG. 6. Frequency distribution function of hcp He^4 at $V_m = 16.00$ cm^3 calculated using the 18-parameter force-constant model which was fitted to the dispersion curves.

sociated with the onset of melting. We have also used the force-constant model to calculate the basal plane and the c-axis Debye-Waller factors as defined in Eq. (2). The functions $G_{\parallel}(T/\Theta_0)$ and $G_{\perp}(T/\Theta_0)$ are tabulated in Table IV. At $T = 4$ K, we have $G_{\parallel} = 6.366$ and $G_{\perp} = 7.906$, resulting in a rather large anisotropy of 20%.

The motivation for using the force-constant model as an interpolation scheme to calculate thermodynamic properties of hcp He^4 was that in view of the scaling of the frequencies with molar volume, the above calculations may in principle be used to predict such thermodynamic properties over a wide range of molar volumes. For instance, both the (Θ_D/Θ_0) vs (T/Θ_0) curve and the $G_{\parallel}(T/\Theta_0)$ and $G_{\perp}(T/\Theta_0)$ are universal functions independent of molar volume in this approximation. Nevertheless, it is possible that the model may not correctly represent the off-symmetry-direction dispersion relations, except insofar as they are consistent with C_{13}, and hence must have the correct initial slopes for the acoustic modes.

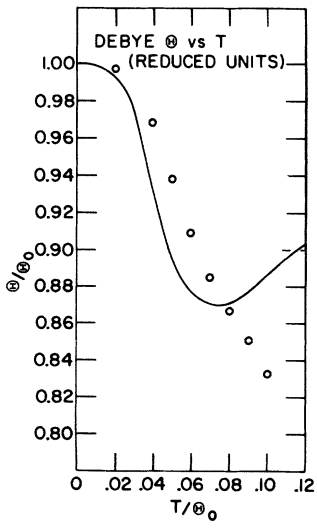

FIG. 7. Plot of reduced Debye temperature vs reduced temperature as measured by Ahlers (Ref. 19) and as calculated from our frequency spectrum. Θ_0(expt) = 52 K, while Θ_0(calc) = 47.2 K.

TABLE IV. Dimensionless functions $G_{\parallel}(T/\Theta_0)$ and $G_{\perp}(T/\Theta_0)$ appearing in Eq. (6) for the Debye-Waller factor.

T/Θ_0	$G_{\parallel}(T/\Theta_0)$	$G_{\perp}(T/\Theta_0)$
0.04	3.126	3.894
0.06	4.727	5.879
0.08	6.366	7.906
0.10	8.055	9.998
0.20	17.524	21.950
0.30	29.224	37.360
0.40	43.706	56.901
0.50	61.211	80.855

As mentioned in the Introduction, perhaps the most important aspect of these results together with the Brookhaven data is that they provide the first detailed check of the self-consistent phonon theory and its density dependence. The lattice dynamics of solid helium were treated by GKW on the basis of essentially replacing the usual force constants in the Born–von Karman theory, which are evaluated in terms of the second derivatives of the interatomic Lennard-Jones potential at the equilibrium sites, by such derivatives *averaged* over the ground-state harmonic-oscillator wave function of the system. The hard core of the effective interatomic potential thus obtained is softened by introducing a short-range pair-correlation function in the wave function, i. e., by writing

$$\Psi(\vec{r}_1, \ldots, \vec{r}_N) = \left(\prod_{i<j\leq N} f(\vec{r}_j - \vec{r}_i) \right) \times \Phi(\vec{r}_1, \ldots, \vec{r}_N), \tag{6}$$

where $\Phi(\vec{r}_1, \ldots, \vec{r}_N)$ is the usual ground-state harmonic-oscillator wave function, and the short-range correlation function is written as

$$f(r) = \exp[-\tfrac{1}{2} C v(r)] . \tag{7}$$

In Eq. (7), C is a constant parameter, and $v(r)$ is the Lennard-Jones potential. The effect of $f(r)$ in Eq. (6) is to modify the effective interatomic potential whose second derivative is being averaged, as well as to modify the averaging procedure. Self-consistency is introduced by solving for the eigenvalues of the dynamical matrix and using these eigenvalues in the wave function $\Phi(\vec{r}_1, \ldots, \vec{r}_N)$ in Eq. (6) and redoing the averaging, until the procedure converges. A further complication is introduced by the fact that the scattered neutron groups are peaked at the positions corresponding to the poles of the displacement-displacement correlation function (in the one-phonon approximation) rather

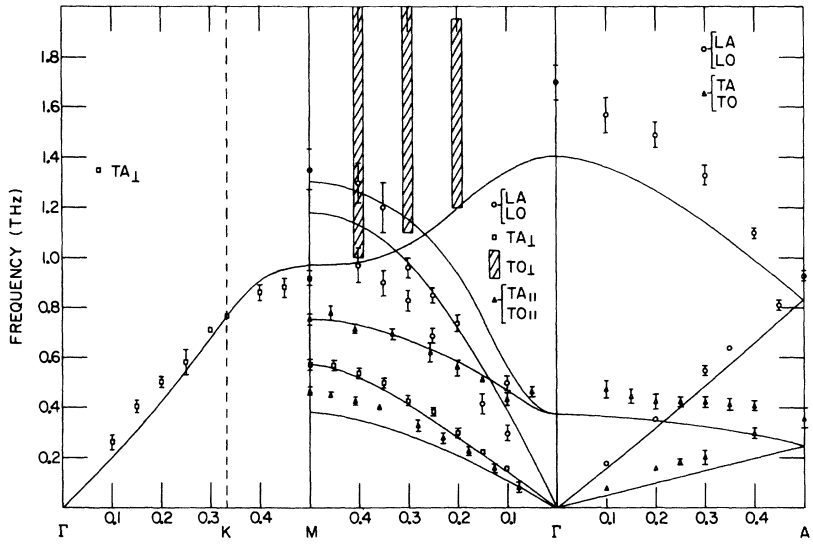

FIG. 8. Experimental dispersion curves for hcp He^4 plotted together with the predictions of the theory of Gillis, Koehler, and Werthamer (Ref. 3) for $V_m = 16.00$ cm^3.

than at the frequencies given by the eigenvalues of the dynamical matrix obtained from these above effective force constants. Full details may be found in the paper by GKW[3] and references therein.

Figure 8 shows the comparison between the GKW calculations for $V_m = 16.00$ cm^3 and our experimental data. As has been noted earlier for the ΓA direction, the calculated curves, although in reasonable agreement with the data, are generally too low compared to the measured frequencies. For this direction, the theoretical curves are about 16% lower than the measured ones. For the ΓM direction, the $\Sigma_4(\mathrm{TO}_\parallel)$ branch (scaled from the 21.2-cm^3 data) is predicted very well by the theory, whereas the theoretical $\Sigma_4(\mathrm{TA}_\parallel)$ is about 15% too low at the zone boundary. The $\Sigma_3(\mathrm{TA}_\perp)$ branch is also in reasonably good agreement, the maximum discrepancy being about 8%. The worst disagreement seems to be for the Σ_1(LA and LO) branches which are, respectively, too *high* by 30 and 21% halfway to the zone edge. This is interesting in view of the fact that all the other theoretical curves lie *lower* than experiment. At the zone edge the theoretical LO branch is in good agreement with the data. For the $T_3(\mathrm{TA}_\perp)$ mode, the maximum disagreement with experiment also appears to be halfway to the zone edge and is about 30%. For the Brookhaven data at $V_m = 21.1$ cm^3, the GKW theory predicted dispersion curves higher than the experimental curves for all the measured modes. Thus it appears that although the theory is in semiquantitative agreement with the data at both molar volumes, its prediction of the volume dependence of the frequencies is not correct.

The intensities associated with some of the Σ_1 branch neutron groups behave somewhat anomalously. For instance, the groups corresponding to the Σ_1 (LO) branch at $\zeta = 0.5$ and 0.4 [$\vec{q} = (4\pi/\sqrt{3}a)(\zeta\ 0\ \bar{\zeta}\ 0)$] have intensities which are not in accordance with the structure factor defined by Eq. (3) and are calculated either from the force-constant model obtained above, or from the eigenvectors obtained from the GKW theory.[3] Figure 9 shows $g_j^2(\vec{Q})$ for the Σ_1 (LO and LA) branches as a function of $\vec{Q}$ as calculated from both the above models. To explain the observed intensities of some of the neutron groups at $\zeta = 0.5$ and $\zeta = 0.4$, one would have to postulate that the $g_j^2(Q)$ for the two branches actually crossed once more before $\vec{Q} = (4\pi/\sqrt{3}a)$ $(1.5,\ 0,\ -1.5,\ 0)$, ending up with LO dominating at the zone boundary. However, it is possible that the anomalous intensities arise because of a multiple (Bragg followed by a one-phonon) scattering process.

Finally, we discuss the anomalous neutron groups

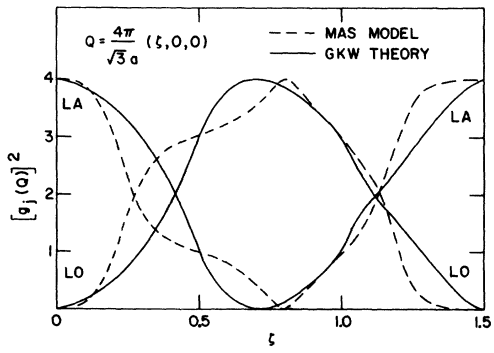

FIG. 9. Plot of the inelastic neutron structure factor squared $|g_j(\vec{Q})|^2$ for the longitudinal modes along Σ as calculated from the empirical force-constant model and from the GKW theory. These are given in units of $b^2(\vec{Q}\cdot\hat{e})^2/M\omega_j^2(\vec{q})$, where $\hat{e}$ is a unit vector along $\vec{q}$.

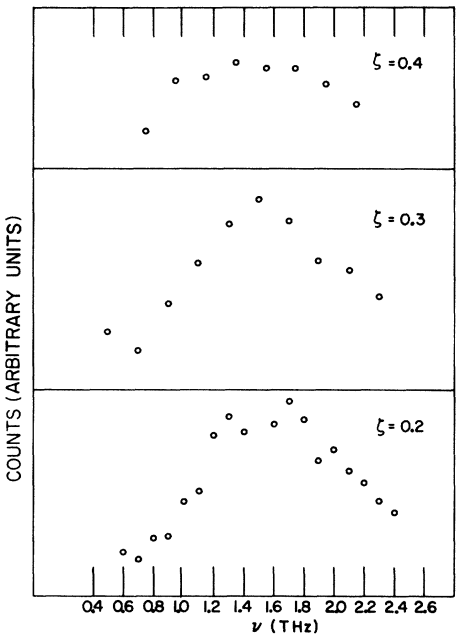

FIG. 10. Anomalously broadened neutron groups observed while searching for $TO_\perp$ branch phonons along Σ.

which were observed while searching for the Σ_3 ($TO_\perp$) branch phonons. Figure 10 shows the neutron groups observed in these scans. It may be seen that they all suffer extreme broadening and in some cases exhibit considerable asymmetry. Because of this broadening, the positions of these phonons have been indicated by cross-hatched bars in the dispersion curve diagram of Fig. 4. Their mean positions correspond to frequencies which are surprisingly high compared to the expected dispersion for the $\Sigma_3(TO_\perp)$ branch, which we note by symmetry must join up with Δ_2 (LO) at Γ and with $T_3(TA_\perp)$ at M. If one is to believe these mean positions, it would imply that the Σ_4 ($TO_\perp$) branch dips abruptly down near the zone edge to join up with T_3 ($TA_\perp$) at M. It is possible that the mean positions of these groups are considerably shifted by damping effects which are beyond the scope of the current theories, and, in fact, it is likely that more refined theories would have to explain the actual neutron group profile rather than simply characterize it by a mean position and a width. As is the case with some of the higher-frequency Δ_2(LO) branch phonons, these neutron groups do not seem to correspond to well-defined excitations. If they are phonons, they would be damped out within one or two oscillations. However, one cannot rule out the possibility that there are other types of excitations in the high-frequency region of the phonon spectrum, including possibly a continuum of single-particle excitations. It should be noted that it is precisely the Δ_2(LO) and $\Sigma_3(TA_\perp)$ branches, which we find greatly damped, that the Brookhaven group was unable to observe at their molar volume.

V. CONCLUSION

We find that for the lower frequencies at least (below 0.8 THz), well-defined phonon-type excitations exist in solid He^4 at a molar volume of 16 cm^3, with no observable natural broadening. The higher-frequency branches of the dispersion curve, including the Δ_2(LO) branch and especially the $\Sigma_3(TO_\perp)$ branch, are subject to considerable damping. Although the intensities of the observed neutron groups drop precipitously as one gets into the higher-frequency modes, due to the $1/\omega$ and Debye-Waller factors in the cross section, nevertheless, there seems to be no pronounced deviation from the conventional one-phonon cross-section formula for neutron scattering. Our intensity measurements are not sufficiently accurate to observe theoretically predicted deviations from this cross section, in terms of a modification of the Debye-Waller factor, as recently proposed by Gillessen and Biem[20] and others. We have obtained a parametrized force-constant model to be used as an interpolation scheme to obtain the phonon frequencies all over the zone. This was useful in characterizing the measured phonon spectrum for solid hcp He^4, enabling other properties, such as structure factors and thermodynamic properties, to be calculated.

It is concluded that further work needs to be done on calculating the damping effects on the self-consistent phonons and perhaps in improving on the short-range correlation effects in the theory, so as to improve on the density dependence of the theoretically predicted phonon frequencies.

ACKNOWLEDGMENTS

We would like to express our appreciation for the continuing advice and encouragement provided by Dr. C. A. Swenson, and our thanks to Dr. T. R. Koehler for sending us details of his calculations of the frequencies and eigenvectors.

*Work performed in the Ames Laboratory of the U. S. Atomic Energy Commission. Contribution No. 2847.

[1]N. R. Werthamer, Am. J. Phys. 37, 763 (1969).
[2]T. R. Koehler, Phys. Rev. 165, 942 (1968).
[3]N. S. Gillis, T. R. Koehler, and N. R. Werthamer, Phys. Rev. 175, 1110 (1968).
[4]L. H. Nosanow, Phys. Rev. 146, 120 (1966).
[5]J. E. Vos, Ph.D. thesis, Technische Hogeschool Delfts, Netherlands, 1968 (unpublished).
[6]W. D. Seward, D. Lazarus, and S. C. Fain, Phys. Rev. 178, 345 (1969).
[7]S. C. Fain and D. Lazarus, Phys. Rev. (to be

published).
[8]J. P. Franck and R. Wanner, Phys. Rev. Letters 25, 345 (1970).
[9]V. J. Minkiewicz, T. A. Kitchens, F. P. Lipschultz, R. Nathans, and G. Shirane, Phys. Rev. 174, 267 (1968).
[10]T. O. Brun, S. K. Sinha, C. A. Swenson, and C. R. Tilford, in *Neutron Inelastic Scattering* (International Atomic Energy Agency, Vienna, 1968), Vol. I.
[11]M. Bitter, W. Gissler, and T. Springer, Phys. Status Solidi 23, K155 (1967).
[12]S. K. Sinha, T. O. Brun, L. D. Muhlestein, and J. Sakurai, Phys. Rev. 31, 2430 (1970).
[13]M. J. Cooper and R. Nathans, Acta Cryst. 23, 357 (1967).
[14]J. F. Jarvis, D. Ramm, and H. Meyer, Phys. Rev. 170, 320 (1968).
[15]C. A. Swenson, J. Phys. Chem. Solids 29, 1337 (1968).
[16]R. E. DeWames, T. Wolfram, and G. W. Lehman, Phys. Rev. 138, A717 (1964).
[17]A. Czachor, in *Inelastic Scattering of Neutrons* (International Atomic Energy Agency, Vienna, 1965), Vol. I.
[18]L. J. Raubenheimer and G. Gilat, Phys. Rev. 157, 586 (1967).
[19]G. Ahlers, Phys. Rev. A 2, 1505 (1970).
[20]P. Gillessen and W. Biem, Z. Physik 216, 499 (1968).

PHYSICAL REVIEW A VOLUME 3, NUMBER 5 MAY 1971

Heat Conduction by Helium II Contained in Small Channels*

E. C. Alcaraz† and H. H. Madden
Department of Physics, Wayne State University, Detroit, Michigan 48202
(Received 15 June 1970; revised manuscript received 28 December 1970)

Helium-II heat-flow experiments have been carried out with the helium contained in small channels (tubes $< 10\ \mu$ in diameter d) having simple geometries and with the temperature differences limited to $\sim 5\times10^{-3}$ K° or less. In this domain, the heat current density is found to be proportional to the temperature gradient and the differential thermohydrodynamic equations of London and Zilsel should be valid. Comparison with the London-Zilsel theory shows good agreement for most of our data with regard to the absolute magnitude of the thermal conductivity κ and its dependence on temperature. The experimental κ values have a weaker dependence on the channel size than the theoretically predicted square of d, and this size dependence is a function of temperature. Our data for the largest channels ($d \sim 8\ \mu$) and at the larger heat current densities depart significantly from the London-Zilsel predictions. This difference is not explainable on the basis of a Gorter-Mellink mutual friction, but is consistent with a dissipative flow for the superfluid depending linearly on its velocity. This superfluid dissipative flow is comparable to that reported in other helium-flow experiments.

I. INTRODUCTION

In the helium-II heat-transfer domain where the simple "internal-convection" mechanism of Tisza[1] and London[2] is the only mechanism to be considered, the heat current density should be proportional to the temperature gradient and a thermal conductivity is definable for the helium II contained in a channel of particular geometry. London and Zilsel[3] have calculated the heat conducted in this domain by helium II contained in a cylindrical capillary of diameter d and find a mean thermal conductivity given by $(\rho s)^2 T d^2/32\eta_n$, where ρs is the entropy density of helium II, T is the temperature, and η_n is the viscosity of the normal fluid. Experiments have been carried out in our laboratory in an attempt to test the theoretical results of London and Zilsel. In order to do this, small channels with diameters of less than 10 μ were used and the temperature gradients were restricted to values less than 3×10^{-3} °K/cm. Our earlier results,[4] while showing linear heat-current-density–temperature-gradient relationships, were complicated by an apparent dependence of the thermal conductivity on the length of the capillaries, similar to the length effect discussed by London and Zilsel[3] and reported by Forstat.[5] Those results have now been found to be spurious and related to defects in the channels used in our earlier experiments.[6] The results presented below have been obtained using new channels in which any defects present play a minor role in the heat-conduction process. The bulk of our new data shows good agreement with the London-Zilsel theory, with no apparent thermal-conductivity length effect. For our largest channels and at the highest heat current densities, however, the results depart significantly from the London-Zilsel prediction. This departure seems not to be related to the nonlinear behavior associated with mutual friction[7] but may be interpreted in terms of a dissipative flow of the superfluid depending linearly on its velocity.

Two successful attempts, utilizing well-defined channels of simple geometry, to verify the thermal-conductivity expression of London and Zilsel have

FIG. 1. Photograph of the helium crystal used in most of the measurements taken by Bragg reflection of neutrons.